Correspondence to:
A. Ampuero,
angelaampuero@id.uff.br
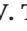
The Forest Effects on the Isotopic Composition of Rainfall in the Northwestern Amazon Basin

A. Ampuero[1] , N. M. Stríkis[1] , J. Apaéstegui[2] , M. Vuille[3] , V. F. Novello[4] , J. C. Espinoza[5] , F. W. Cruz[4] , H. Vonhof[6] , V. C. Mayta[7] , V. T. S. Martins[4] , R. C. Cordeiro[1] , V. Azevedo[1] , and A. Sifeddine[8]

[1]Departamento de Geoquímica, Universidade Federal Fluminense, Niterói, Brazil, [2]Instituto Geofísico del Perú, Lima, Peru, [3]Department of Atmospheric and Environmental Sciences, State University of New York at Albany, Albany, NY, USA, [4]Instituto de Geociência, Universidade de São Paulo, São Paulo, Brazil, [5]Université Grenoble Alpes, IRD, CNRS, Grenoble INP, Institut des Géosciences de l'Environnement (IGE, UMR 5001), Grenoble, France, [6]Department of Climate Geochemistry, Max Planck Institute for Chemistry, Mainz, Germany, [7]Departamento de Ciências Atmosféricas, IAG, Universidade de São Paulo, São Paulo, Brazil, [8]IRD-Sorbonne Universités (UPMC, CNRS, MNHN), UMR LOCEAN, Centre IRD, Bondy, lFrance

Abstract In the Amazon basin, intense precipitation recycling across the forest significantly modifies the isotopic composition of rainfall (δ^{18}O, δD). In the tropical hydrologic cycle, such an effect can be identified through deuterium excess (dxs), yet it remains unclear what environmental factors control dxs, increasing the uncertainty of dxs-based paleoclimate reconstructions. Here we present a 4-year record of the isotopic composition of rainfall, monitored in the northwestern Amazon basin. We analyze the isotopic variations as a function of the air mass history, based on atmospheric back trajectory analyses, satellite observations of precipitation upstream, leaf area index, and simulated moisture recycling along the transport pathway. We show that the precipitation recycling in the forest exerts a significant control on the isotopic composition of precipitation in the northwestern Amazon basin, especially on dxs during the dry season ($r = 0.71$). Applying these observations to existing speleothem and pollen paleorecords, we conclude that winter precipitation increased after the mid-Holocene, as the expansion of the forest allowed for more moisture recycling. Therefore, forest effects should be considered when interpreting paleorecords of past precipitation changes.

Plain Language Summary How forest evapotranspiration affects rainfall and how the forest changes during the Holocene affected the hydrologic cycle of the Amazon basin are fundamental questions that have guided the paleoclimate research in South America. The interplay between precipitation and the forest is potentially archived in the oxygen (δ^{18}O) and hydrogen (δD) isotopes of past rainfall. Following this idea, we explore the use of oxygen and hydrogen isotopes from rainfall as natural markers of moisture recycling. By comparing the water rainfall isotopes with variations of precipitation recycling along the moisture flux pathways, we find that seasonal changes are related with variation in the deuterium excess. Using isotope records from fossil rainwater trapped in cave mineral deposits, known as speleothems, we establish a relationship between vegetation shifts and moisture recycling in the Amazon rainforest during the last 10,000 years. During the Holocene, periods of forest expansion portrayed in pollen records from lakes sediments match with changes in deuterium excess recorded in speleothems from the western Amazon. Our results show that in the Amazon basin forest expansion went hand in hand with moisture recycling.

1. Introduction

The effects of rainforest evapotranspiration on the stable isotopic composition of rainfall (δ^{18}O, δD) are particularly important to reconstruct the hydroclimate history in South America and improve our understanding of the role of the rainforest in the regional hydrological cycle. In general, the isotopic composition of a precipitating air mass moving over a continental area results from a combination of processes that mediate the Rayleigh distillation. In the moist air mass, Raleigh distillation is the process where heavy isotope species are progressively removed from the atmosphere through precipitation, leaving the remaining vapor depleted in heavy isotopes (Vuille & Werner, 2005; and many others). While the progressive condensation of moisture leads to a gradual lowering of heavy isotopes in the remaining vapor, forest-driven processes can reintroduce these heavy isotopes to the atmosphere through evapotranspiration.

The seasonal precipitation over large parts of the Amazon region is mainly characterized by wet conditions in the austral summer, associated with the active phase of the South American Monsoon System (Vera et al., 2006; Zhou & Lau, 1998) and a dry season in austral winter, in the absence of the South American Monsoon System forcing. Moreover, several studies have shown that the Amazon basin itself constitutes a major moisture source for the region, driven by the hydrologic regime of the rainforest (Builes-Jaramillo & Poveda, 2018; Drumond et al., 2014; Molina et al., 2019; Salati et al., 1979). In fact, the forest induces dry season rainfall, necessary to sustain itself when oceanic moisture supply is limited (Staal et al., 2018). Recently, Staal et al. (2018) estimated that about 32% of Amazonian rainfall originates from evapotranspiration within the basin, two thirds of which originate as tree transpiration. The positive feedback between the forest and rainfall promotes cascades of recycled moisture that precipitate across distant areas, allowing for forest cover expansion and playing a significant role in the maintenance of the northwestern Amazonian forest (Staal et al., 2018; Zemp et al., 2014).

A proxy suitable to describe the hydrologic cycling of moisture is deuterium excess (dxs $= \delta D - 8 \times \delta^{18}O$) (Dansgaard, 1964), a second-order parameter derived from kinetic fractionation of the water stable isotopologues. The dxs value of an air mass is influenced by the physical conditions at the oceanic moisture source, principally relative humidity and sea surface temperature (Pfahl & Sodemann, 2014). Moreover, prevailing conditions during advection across the continent and interaction or mixing with different air masses further modify dxs (Froehlich et al., 2002; Gat et al., 1994). Particularly, over large continental areas, such as the Amazon basin, variations in the dxs composition have the potential to serve as a fingerprint of recycled air moisture (Gat et al., 1994; Salati et al., 1979).

Water isotopologue data across the Amazon suggest that changes in forest vegetation may affect the dxs values through changes in the rates of moisture recycling associated with forest evapotranspiration (Salati et al., 1979; Zemp et al., 2014). Evapotranspiration includes two main process: the evaporation from open water, soil, and canopy and the transpiration, which is the biological evaporation trough the leave stomata. Plant transpiration is thought to be a nonfractionation process (Zimmermann, 1967; Koster et al., 1993; Gat et al., 1994), so that the isotopic composition of the transpired water vapor is similar to the isotopic composition of the water in the plant xylem (Farquhar et al., 2007; Griffis et al., 2010; Wang et al., 2012). On the other hand, evaporation, particularly under unsaturated air conditions, fractionates the isotopes of hydrogen and oxygen, resulting in the higher dxs values of evaporated water (Froehlich et al., 2002; Gat et al., 1994). Therefore, dxs can potentially be used as an index for admixture of evaporated moisture. Precipitation from air masses that have undergone considerable incorporation of evaporated water will present higher dxs values.

Although progress has been made in understanding the major drivers of $\delta^{18}O$ and δD variability in tropical regions, the relationship between moisture recycling and the rainfall isotopic composition in the Amazon basin is not fully understood. Moreover, the climatic significance of dxs values over continental areas in the tropics is still unclear (Landais et al., 2010; Risi et al., 2013; Vuille, 2018). In this sense, it is important to clarify the effect of land-atmosphere interactions on the isotopic composition of rain to reliably interpret isotope-based paleoclimate records. For instance, in the Amazon basin paleoprecipitation reconstructions based on speleothem $\delta^{18}O$ records are controversial. Some authors sustain the notion that during the Last Glacial Maximum a strong east-west rainfall isotope gradient along the Amazon basin may have resulted from reduced water recycling, as consequence of a widely drier Amazonia, leading to reduced plant transpiration (Wang et al., 2017). On the other hand, other authors claim that the spatial variability in the isotope rainfall composition resulted from an east-west precipitation dipole (Sylvestre et al., 1999; Cruz et al., 2009; Cheng et al., 2013) associated with an upper-level atmospheric wave response to enhanced monsoon circulation, known as the Bolivian High-Nordeste Low system (Chen et al., 1999; Lenters & Cook, 1997, 1999; Sulca et al., 2016). In this scenario, the increased convective activity and precipitation over the tropical Andes and western Amazon is balanced by enhanced subsidence over Northeastern Brazil, leading to an antiphased precipitation pattern between the western and eastern Amazon, rather than pervasive dry conditions.

Here we take an empirical approach to assess the forest-related influence on rainfall $\delta^{18}O$ and dxs variations. Our analyses rely on $\delta^{18}O$ and dxs data obtained from rainfall monitoring over the western Amazon, climatic and land-surface data derived from satellite observations, and reanalysis data sets. We describe the transport

history of air masses using air parcel back trajectory modeling. Finally, we discuss the paleoclimate implications of dxs variability during the Holocene based on published speleothem and pollen records from continental lake cores.

2. Data and Methodology

2.1. Isotope Monitoring

We used rainfall $\delta^{18}O$ and δD data from a monitoring network installed at the Palestina station (5.92°S, 77.35°W, 870 m. a. s. l.), near the Nueva Cajamarca district, in the Peruvian Region of San Martin, on the eastern flank of the Andes (Figure 1a). Present-day mean annual temperature is ~22.8 °C and mean annual precipitation is ~1,570 mm (Apaéstegui et al., 2014). Precipitation corresponds to a tropical regime with a marked precipitation peak in March and a dry season from July to August (precipitation <100 mm month^{-1}) (Figure 1c). Because dry season precipitation is significant at Palestina station, contributing around 22% of annual precipitation (Figure 1b), it is important to consider its influence on the mean annual $\delta^{18}O$ and dxs composition of rainfall.

The data cover three periods from June 2012 to September 2013 (Apaéstegui et al., 2014), from October 2013 to June 2014 and from October 2016 to June 2018 (Table S1 in the supporting information). Our samples were collected twice a month from a tube-dip-in-water collector with pressure equilibration using 8-ml HDPE and glass bottles. Water isotope analyses were performed at the Centro de Pesquisas de Águas Subterrâneas at the University of São Paulo (IGc-USP), a Laser absorption spectrophotometer of the brand PICARRO L2130i. Data were processed by LIMS for Lasers software (Coplen, 2000; Coplen & Wassenaar, 2015). Values are reported with an analytical precision of 0.09‰ for $\delta^{18}O$ and 0.9‰ for δD relative to Vienna Standard Mean Ocean Water.

2.2. Regional Climate Data

Satellite-derived precipitation data from two products were used. We derived daily precipitation data from the Tropical Rainfall Measuring Mission (TRMM) product 3B42 (Huffman et al., 2007) for the period May 2012 to March 2014 and complemented it with data from the Global Precipitation Measurement (GPM) mission until June 2018. GPM data were spatially interpolated from 0.1° to 0.25°, so they match TRMM data.

To represent the structure of the forest canopy, we used data on leaf area index (LAI), which is a dimensionless variable that refers to the area of photosynthetic tissue per unit ground surface area. LAI is derived from measurements made by the Moderate Resolution Imaging Spectroradiometer (MODIS), on board the National Aeronautics and Space Administration's Terra and Aqua satellites. The product we used is MCD15A2H version 6 MODIS Level 4, which reports values at a spatial resolution of 500 m (Myneni et al., 2015). Retrievals are obtained every 8 days, by averaging the best quality values. To minimize biases, we screened the low-quality data pixels before spatially interpolating the data to a 0.25° grid (see Text S1).

There is still debate about the interpretation of LAI regarding the apparent greening in the Amazon during the dry season. Morton et al. (2014) argued that the apparent greening in the Amazon observed in optical remote sensing data is an artifact of variations in the Sun-sensor geometry and conclude that moisture availability governs photosynthetic activity. On the contrary, Saleska et al. (2016) contend that during normal years sunlight, rather than water, is the limiting control on the photosynthetic activity. This latter notion is supported by evidence based on modeling and field observations, which indicate that in the Amazon, LAI seasonality identified with MODIS is real, but the amplitude of the seasonal changes might not yet be precise. Furthermore, a comprehensive analysis of LAI is reported in Myneni et al. (2007), where the authors analyze the bias of the database, showing its consistency and documenting a strong relationship between LAI and evapotranspiration.

We calculated precipitation recycling (PR) using the Eulerian atmospheric moisture tracking model WAM-2layers (Water accounting model-two layers) version 2.4.8 (van der Ent, 2014). We ran the model with data from the European Centre for Medium-Range Weather Forecasts (ECMWF) Interim Re-Analysis (ERA-Interim) (Dee et al., 2011), on a 1.5° grid. The result in each grid cell (region) represents the ratio of precipitation that originates from land evaporation, either in the same or another continental region, with respect to the total precipitation in the target region. The mean annual and seasonal PR are shown in Figure S1.
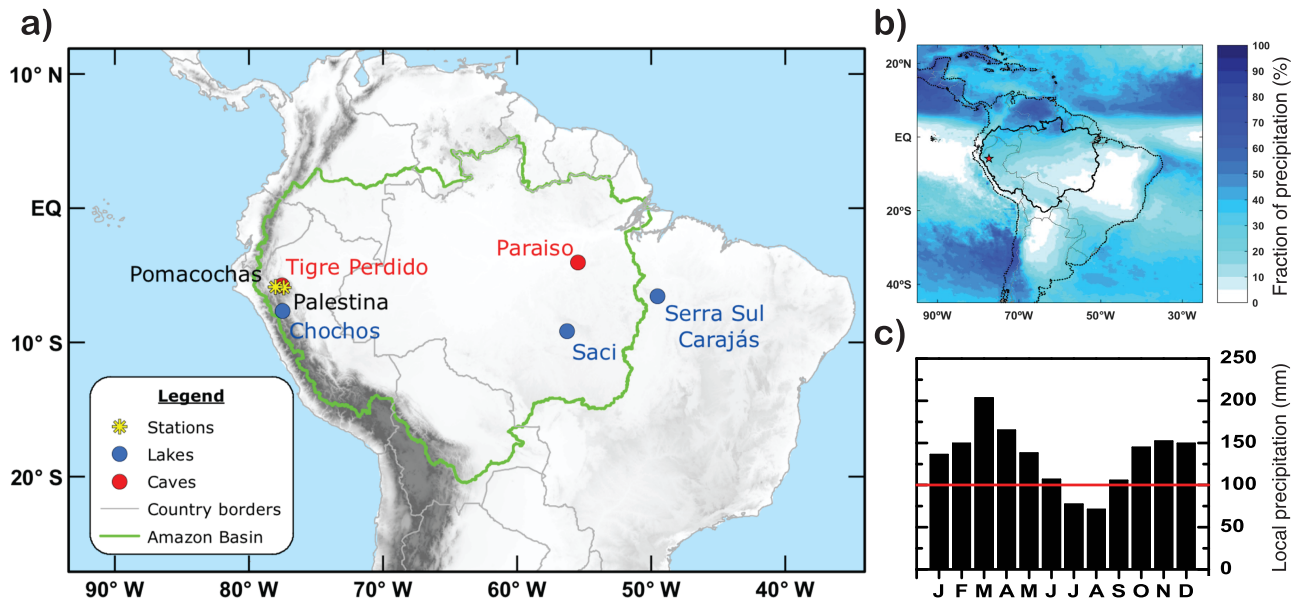
Figure 1. (a) Geographic location of the monitoring stations, caves, and lakes referenced in this study. The dark gray shading represents the Andes mountain range, and the green line highlights the limits of the Amazon Basin taken from the HyBAM data base. (b) Fraction of annual precipitation that corresponds to the period from June to September (extended dry season). (c) Local precipitation at the Palestina location. Panels (b) and (c) were computed for the period from 1998 to 2013 with data from TRMM3B43.

2.3. Palynological Records

A rain forest index was calculated based on available pollen frequency records from three lakes in the eastern and western parts of the Amazon basin: Laguna Chochos, Peru (Bush et al., 2005); Saci, central-south Amazon (Fontes et al., 2017); and Serra Sul Carajás Lake, CSS2 (Absy et al., 1991; Sifeddine et al., 2001) (Figure S2). The records were interpolated in time in order to calculate the spatial average across the three lakes. The geographic location of the lakes in shown in Figure 1a.

2.4. Deuterium Excess Record

Fluid inclusions are microscopic water-filled cavities enclosed in crystals of many minerals. In the speleothems, the fluid inclusions retain the water from the time of mineral formation, thus recording variations of the fossil dripwater (Schwarcz et al., 1976; Van Breukelen et al., 2008). In humid tropical climate the isotope composition of the cave drip water is in equilibrium with local rainfall (Lachniet, 2009; Wackerbarth et al., 2012). Thus, to assess the variation of dxs from past rainfall, a record of dxs from northwestern Amazonia was calculated based on the isotope data of $\delta^{18}O$ and δD from fluid inclusion of speleothems from Tigre Perdido cave (Van Breukelen et al., 2008). Located close to the Palestina station, near the town of Nueva Cajamarca, the speleothem record from Tigre Perdido cave spans the last 13,000 years.

2.5. Methods

Local daily precipitation was estimated based on TRMM and GPM products. To obtain the local precipitation values, the average of 25 tiles was calculated, considering the tile over the Palestina station in the center and the adjacent tiles around it. Since each tile encompasses $0.25° \times 0.25°$, the local precipitation was computed over an area of $1.25° \times 1.25°$.

We modeled air parcel back trajectories with the HYbrid Single-Parcel Lagrangian Integrated Trajectory 4 (HySPLIT 4) model (Stein et al., 2015; Rolph et al., 2017). The model was run with wind fields from ERA-Interim on native spatial resolution of 0.75°. We tracked air parcels back in time for 7 days. As 10 days is the mean residence time of water vapor in the atmosphere (Numaguti, 1999), we consider that 7-day back trajectories cover an air mass pathway back to the point of last saturation and hence the relevant isotopic fractionation processes along the atmospheric moisture transport (Hurley et al., 2012). Back trajectories were initiated at the Palestina station at 500, 1,000, 1,500, and 2,000 m above ground level (m.a.g.l.), representing the boundary layer (e.g., Fisch et al., 2004) and lower troposphere where the main moisture transport

to our study site takes place. Back trajectories were computed every 6 hr at 0, 6, 12, and 18 UTC from May 2012 to May 2018. To assess atmospheric transport variability, we performed cluster analysis of the back trajectories with the package included in HySPLIT4. This cluster analysis technique is more accurate than the monthly clustering because low-level large-scale circulation in the Amazon varies on intraseasonal time scale (e.g., Mayta et al., 2019; Paccini et al., 2017). While a certain circulation pattern may be more frequent during one season, it can appear during other periods of the year as well. With the 6-hr cluster analysis it is possible to group and visualize the back trajectories more clearly than with the monthly approach. Moreover, each back trajectory is tagged with the corresponding cluster number, allowing the calculation of frequency of occurrence of each cluster. It is also possible to relate each trajectory with the amount of local rainfall that fell on the starting day of the back trajectory. Based on this association, the amount of local rainfall that co-occurs with each back trajectory was estimated. For practical reasons, we present only clusters of back trajectories initiated at 1,500 m.a.g.l., at 12 UTC, as considering other heights and times led to similar results (Figure S3). Furthermore, 1,500 m.a.g.l. represents the lower atmosphere where the most significant moisture transport takes place and corresponds to the pressure level where active convection is related to rainfall events over this region (see Segura et al., 2019).

For each cluster, we made composites of low-level wind circulation at 850 hPa and Vertically Integrated Divergence of Moisture Flux from ERA-Interim. Thereby, we directly observe the regional atmospheric circulation patterns that are most influential for our monitoring site and the moisture flux divergence related to each cluster.

All the climate data were summed up along the path of the back trajectories, excluding grid cells over the ocean. In this way, we computed indices of degree of rainout upstream (DRU), accumulated LAI upstream, and PR upstream on a daily time step. These indices represent the state of the forest cover and the atmospheric processes along the air mass pathways to our monitoring site. A similar approach has been used in other studies (Baker et al., 2016; Fiorella et al., 2015). Daily indices were averaged across the four vertical levels mentioned above. To better assess the effect of these indices on the isotopic signature, all values were weighted by local precipitation in 2-week time steps, which is the frequency of the water isotopologue sampling. This approach permits us to better estimate the extent to which the indices affect the isotopic values of rainfall at the monitoring site. For instance, by weighting DRU by the local precipitation, a high value of DRU associated with an event of reduced local precipitation will have a minor importance given that it corresponds to a small fraction of the total water that reached the study site. Hence, this approach allows us to estimate how much of the isotopic signals can be related to DRU, LAI, and moisture recycling upstream of our study site. Finally, for comparisons between the indices and the isotopic data, seasonality of each variable was removed. For more details about the computation of the indices; see Text S1.

3. Results

3.1. Precipitation and Back Trajectory Analysis

Trade winds dominate large-scale atmospheric transport in tropical South America, varying from northeastern direction during austral summer to southeastern direction during austral winter. Eleven clusters of back trajectories summarize the atmospheric transport to the monitoring site (Figure 2).

Most of the local precipitation can be associated with three groups of clusters. Air masses crossing the Amazon basin (Clusters 2, 3, 4, 6, and 7) are associated with 40% of annual rainfall at the collecting site. These clusters are frequent during austral winter times and are characterized by neutral conditions, meaning that neither convection nor advection dominates, to moisture advective conditions over the central Amazon and convection at the monitoring site. Moreover, 34% of the local precipitation results from northeastern trajectories (Clusters 1, 5, and 11) that are frequent during austral summer. A smaller portion of 14.5% of the local precipitation results from short-length trajectories (Cluster 8) that appear to be related to regional- to local-scale transport and are frequent around the equinoxes.

Although trajectories originating over the Pacific Ocean (Cluster 10) account for 8.5% of the annual rainfall, it is unlikely that those air masses transport moisture across the Andes. Although air masses can cross the Andes from west to east, cold sea surface temperatures and air masses over the eastern Pacific Ocean limit evaporation; thereby inhibiting moisture transport (Houze, 1993). Instead, associated precipitation likely
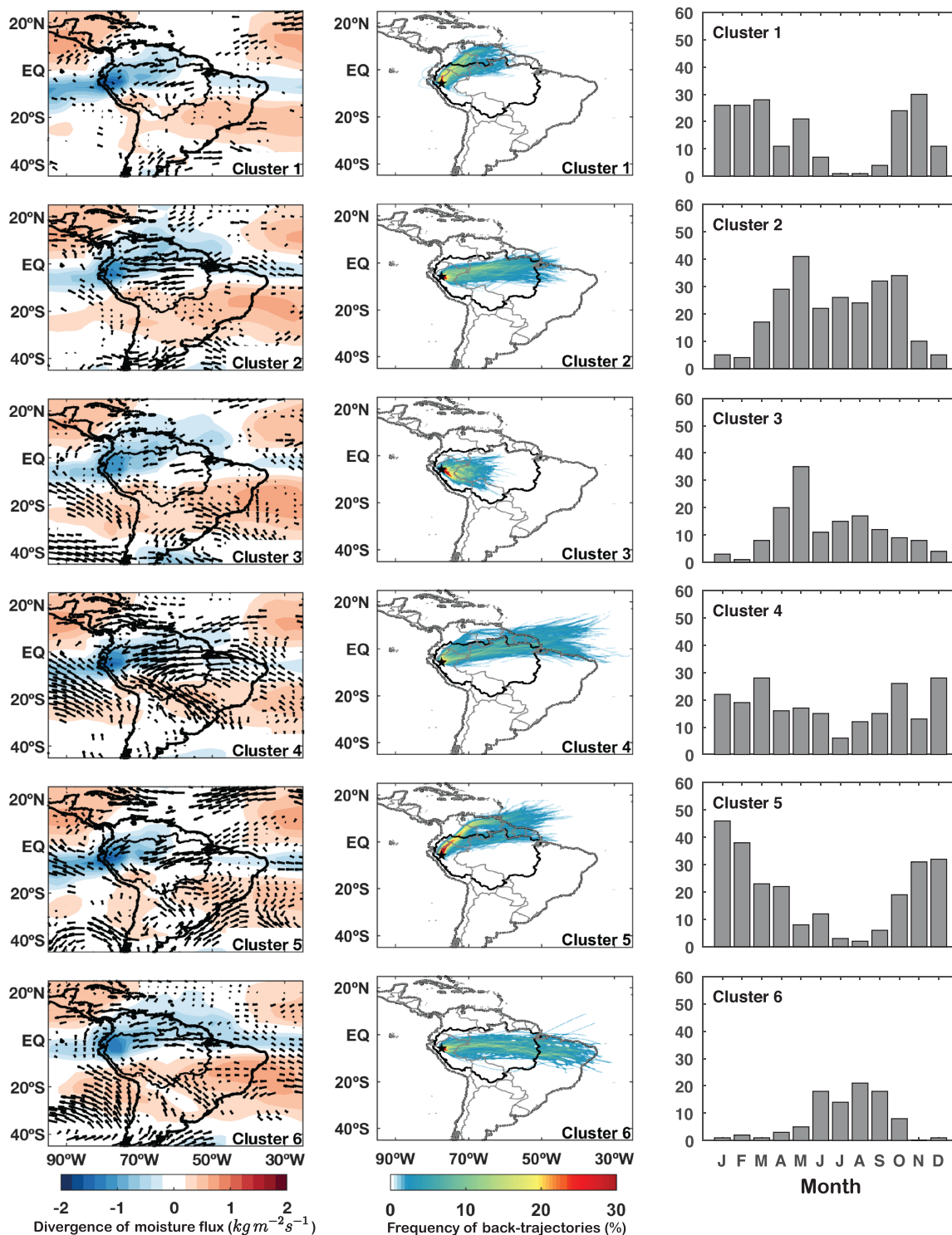
Figure 2a. Low-level wind circulation, moisture flux divergence, and clusters of back trajectories from June 2012 to May 2018. The left column shows the composite maps of the vertically integrated moisture-flux divergence and winds at 850 hPa associated with the clusters. Shaded divergence anomalies in 10^{-5} kg m^{-2} s^{-1} were computed for the same period as the clusters. Vectors are plotted only where either the u or v component is significant at the 95% level, with the largest vectors around 2 m s^{-1}. The central column shows the clusters of 7-day back trajectories at 1,500 m.a.g.l. Shading indicates the percentage of back trajectories passing over each grid cell. If all the back trajectories in one cluster pass over the same grid cell, it would have a value of 100%. To improve visibility of the results, the color scale only covers the range from 0% to 30%. The black star marks the location of the Palestina station. The right column shows the number of back trajectory clusters per month.
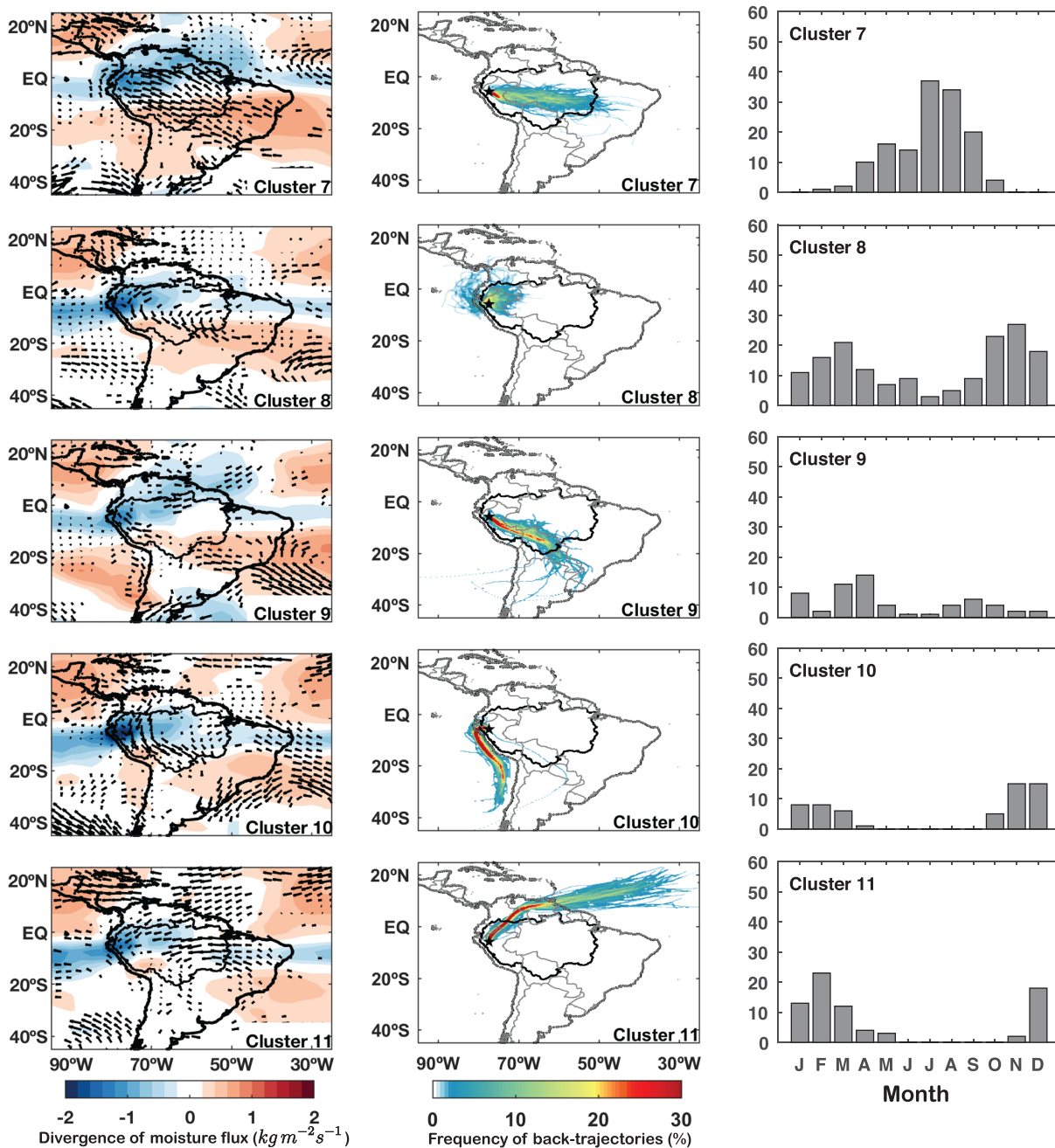
Figure 2b.

results from local moisture. Precipitation associated with extratropical fronts, known to significantly affect precipitation in the south-central Peruvian Andes and Amazonia (Espinoza et al., 2013; Hurley et al., 2015), is associated with the remaining 3% of local rainfall (Cluster 9); however, Cluster 7 that predominates during the austral winter (when extratropical fronts are more frequent) shows a clear southern component and is probably also influenced by extratropical cold air incursions into the Amazon basin.

In general, the DRU annual cycle is similar to the one of local precipitation, although there is an offset from March to July (Figure 3a). The differences become larger on shorter time scales; in fact, at biweekly time steps DRU and local precipitation are correlated with $r = 0.51$, $p < 0.01$. Those differences arise because
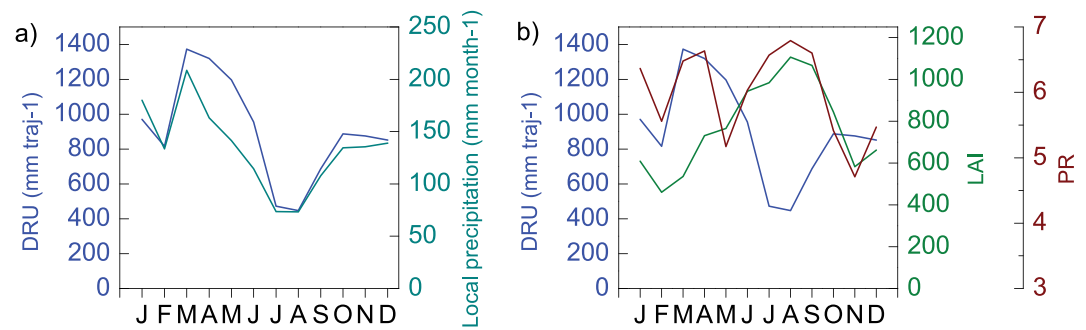
Figure 3. (a) Annual cycle of the degree of rainout upstream (DRU) and local precipitation from 2012 to 2018. DRU is the accumulated precipitation along the back trajectories that initiate on precipitation days at the Palestina station. Local precipitation is calculated from TRMM3B42 and GPM by averaging the nearest tiles to the Palestina station. (b) Annual cycle of the degree of rainout upstream (DRU), leaf area index along the back trajectories (LAI), and precipitation recycling along the back trajectories (PR) for the period from June 2012 to May 2018.

DRU integrates areas with different precipitation regimes across the continent, while local precipitation reflects only the local regime.

3.2. Forest Moisture Fluxes

Accumulated LAI values along the back trajectories present the lowest values in February and increase continuously until reaching a peak around August and September (Figure 3b). Although cloud cover during the rainy season might lead to underestimation of LAI values, thereby resulting in a negative relationship with precipitation, LAI is not consistently correlated with DRU. This could be related to the fact that the main moisture transport to our monitoring site does not consistently cross the region of most intense convection upstream. For instance, during austral summer, the strongest convection is located over the central and southern parts of the Amazon basin, while advection to our site occurs farther north. The opposite is true during austral winter. These observations based on our back trajectory approach suggest that DRU and LAI vary independently from one another.

PR along trajectories was also analyzed. It is worth noting that PR and LAI display similar characteristics during the dry season and the beginning of the wet season and also vary in the same way as with precipitation during the wet season (Figure 3b). Although PR depends on both precipitation and evapotranspiration, during the dry season, evapotranspiration becomes more important. It makes sense that the lowest PR values appear during austral summer, when the moisture influx from the tropical north Atlantic is at its maximum (Clusters 1, 5, and 11 in Figure 2), and the highest PR values occur at the end of the dry season, when evapotranspiration in the Amazon is the highest (Sörensson & Ruscica 2018).

3.3. Isotope Monitoring

The isotopic composition of the local precipitation fits well with the Global Meteoric Water Line (Figure 4a), presenting a slope of 8.40 and an intercept (dxs) of 16.74. The $\delta^{18}O$ values range from $-18‰$ to $0‰$. The most isotopically depleted rainfall occurs in in March–April–May (Figure 5a), consistent with the contribution of moisture from the ITCZ region, which is depleted compared with the other sources (see Rozanski et al., 1993). dxs values range from $8.4‰$ to $20.4‰$, with the highest values in July–August–September (Figure 5b) and higher natural variability than its analytical uncertainty ($0.94‰$). During the study period, dxs and $\delta^{18}O$ show a positive correlation ($r = 0.51$, $p < 0.01$; Figure 4b) whereby dxs increases in relation to $\delta^{18}O$ at about $0.40‰$, on a biweekly time step (Figure 4b). This slope is high compared with the global average, although the latter value of 0.1–0.2 is based on long-term annual averages from GNIP stations (Froehlich et al., 2002).

Although $\delta^{18}O$ is an intrinsic parameter in the calculation of dxs and they are directly correlated, significant differences arise between their values in response to distinct land-atmosphere processes. Table 1 summarizes the linear correlation coefficients (r values) between the isotope values of $\delta^{18}O$ and dxs with the local precipitation at the monitoring site and calculated parameters in the back trajectories (DRU, LAI, and PR) with seasonality removed (Figure 6). The original time series, before removing seasonality, is shown in Figure S4.
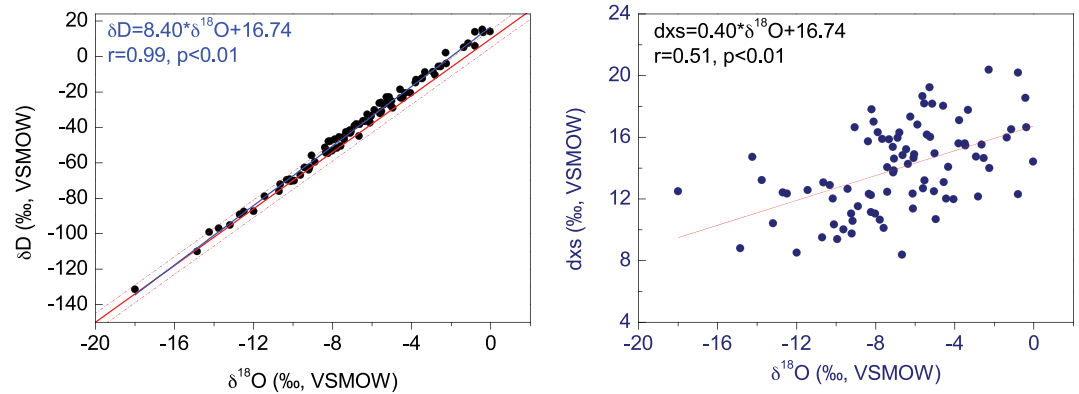
Figure 4. (a) δ^{18}O and δD of precipitation at the Palestina station on a bi-weekly time step. The GMWL is represented by a solid red line and deviations of $\pm 5\permil$ are represented with dashed lines. (b) Correlation between of δ^{18}O and dxs of precipitation at the Palestina station on a bi-weekly time step.

At the monitoring site, the main control on δ^{18}O is DRU ($r = -0.21$, $p < 0.10$), while no significant correlation with local precipitation is observed. This result confirms that DRU, which represents the air mass precipitation history, is a more accurate metric of the physical processes affecting the isotopic fractionation than the simple local precipitation amount (Konecky et al., 2019). On the other hand, dxs shows the best positive correlation with PR ($r = 0.28$, $p < 0.05$).

Furthermore, when we separately analyze extended dry season (June to September [JJAS]) and rainy season (October to February [ONDJF] and March to May [MAM]), we find a strong correlation between δ^{18}O and DRU ($r = -0.67$, $p < 0.05$) and a weaker correlation with local precipitation ($r = -0.39$, $p < 0.10$) during the dry season. During the same period, dxs shows significant positive correlations with LAI and PR ($r = 0.49$ and 0.71 respectively, $p < 0.05$). Conversely, during the rainy season no significant correlations appear between δ^{18}O and the considered parameters. However, there is a significant correlation between dxs and PR during ONDJF ($r = 0.36$, $p < 0.05$) and between dxs and local precipitation during MAM ($r = 0.45$, $p < 0.05$). Table 2 summarizes the correlation coefficients.

4. Discussion

The Amazon basin leaf area observations during our monitoring period (2012–2018) show a consistent seasonality, with values that are on average 20% higher during the dry season than during the wet season. These results are consistent with previous findings (Myneni et al., 2007). Moreover, based on the values calculated from the back trajectories, LAI and PR are characterized by a remarkably consistent increase of about 140% and 44%, respectively, during the dry season. The forest leaf area exerts a strong control on moisture exchange between the forest and the atmosphere, with the potential to affect isotopic fractionation over the Amazon basin.

4.1. Controls on δ^{18}O and Dxs in Precipitation

Table 1
Linear Correlation Coefficient (r) Between Isotope Records and Potential Climatic Controls Based on Biweekly Data

Parameters	δ^{18}O	dxs
Local precipitation	−0.10	−0.01
DRU	*−0.21*	−0.18
LAI	0.06	0.15
PR	0.04	**0.28**

Note. Seasonality was removed from all time series. The r values are shown in bold (if $p < 0.05$) and in italics (if $p < 0.10$).

The processes that involve isotopic fractionation are associated with climatic conditions, which vary seasonally at our study site. Furthermore, the seasonality of the isotopic and climatic indices is strong enough to mask the actual correlation between them. Therefore, it is important to analyze the entire time series to obtain a comprehensive view of the correlations between the data and to analyze each season independently in order to set apart the dominant climatic processes.

When analyzing the complete time series, the negative correlation between δ^{18}O and DRU reflects the removal of heavy isotopic species through precipitation during air mass transport as in a Rayleigh
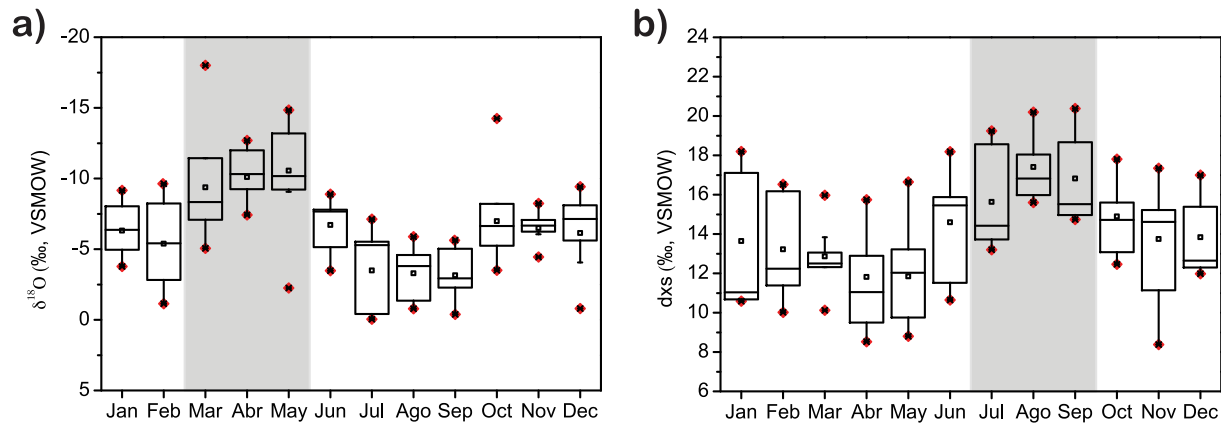
Figure 5. Boxplot of monthly (a) $\delta^{18}O$ and (b) dxs of precipitation at the Palestina station based on biweekly sampling.

model. The correlation with DRU is stronger than with local precipitation, suggesting that at the monitoring site, a strong local influence on the isotopic composition of rainwater can be ruled out. This result is consistent with previous studies from the eastern flank of the Andes, where regional precipitation and large-scale atmospheric transport are considered the main drivers on $\delta^{18}O$ (Vimeux et al., 2005; Villacís et al., 2008; Insel et al., 2013; Windhorst et al., 2013; Fiorella et al., 2015, Samuels-Crow et al., 2014; Hurley et al., 2015). We also assume that below clouds, secondary evaporation has a negligible effect at our study site, given that frequent heavy rainfall, typical for tropical rain forests, would suppress that effect (Peng et al., 2007).

When considering the seasons separately (Table 2), dxs is highly correlated with PR ($r = 0.71$) and LAI ($r = 0.49$) along the air parcel trajectories during the extended dry season only. As LAI is a good index for evapotranspiration in the Amazon basin (Myneni et al., 2007), we infer that high values of dxs imply an increased contribution of recycled moisture from the forest to precipitation at the monitoring site. Conversely, we find no significant correlation between dxs and LAI during the wet season months (ONDJF and MAM), when back trajectories from the north predominate. Indeed, from back trajectory analysis we know that atmospheric transport from the tropical North Atlantic dominates during the austral summer and precipitation is mostly oceanic in origin (Figure 2). The tropical North Atlantic pathway (Clusters 1, 5, and 11) is characterized by the lowest moisture recycling and contributes nearly 34% of the total annual precipitation falling over our station. During this period, precipitation is not significantly affected by land processes; therefore, resupply of moisture through evapotranspiration is unlikely. The opposite is true for the dry months, when the correlation between DRU and $\delta^{18}O$ increases to -0.67 ($p < 0.05$). The high negative correlation between DRU and $\delta^{18}O$ during the dry season suggests that high moisture recycling across the forest, when the last is a major moisture source, does not necessarily overwhelm the progressive depletion in heavy isotopes dictated by the Rayleigh distillation process. Moreover, results suggest that advection across open forest permits land-atmosphere interactions, such as moisture recycling and large-scale transport. This result, together with the enhanced moisture recycling observed at that time (Figure S1), confirms the seasonal forest influence on dxs.

During the wet months, there are significant correlations between dxs and PR during ONDJF and with local precipitation during MAM ($r = 0.36$ and $r = 0.45$), but they are not as consistent as the observations during the dry months. In the first case, the correlation of dxs with PR is lower than during JJAS and there is no significant correlation with LAI. In the second case, the correlation with local precipitation is positive, which contradicts the physical mechanisms that explain the isotopic fractionation in the region, which are the rainout upstream and the amount effect. The lack of significant correlations and inconsistent results obtained during the

Table 2

As in Table 1 but for Extended Dry Months (JJAS) and Wet Months (ONDJF and MAM)

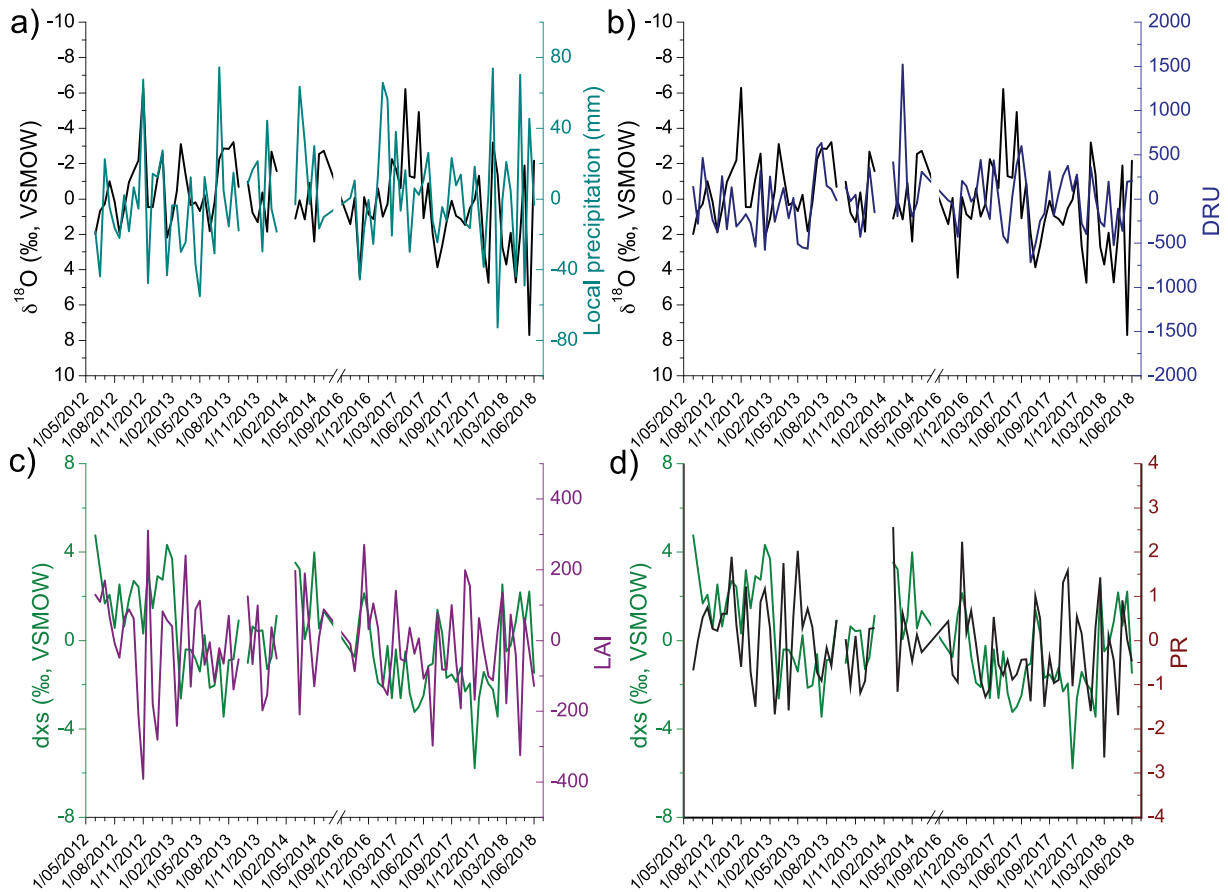| Season	Parameters	$\delta^{18}O$	dxs
JJAS	Local precipitation	−0.39	−0.33
	DRU	**−0.67**	−0.34
	LAI	−0.14	**0.49**
	PR	0.07	**0.71**
ONDJF	Local precipitation	−0.25	−0.12
	DRU	−0.25	−0.25
	LAI	0.25	0.18
	PR	0.03	**0.36**
MAM	Local precipitation	0.23	**0.45**
	DRU	0.01	−0.07
	LAI	−0.15	−0.28
	PR	0.06	−0.12

Figure 6. Records without seasonality (anomalies). Upper panels show δ^{18}O of precipitation and (a) local precipitation accumulated along the water sampling period and (b) calculated degree of rainout upstream (DRU), weighted by local precipitation for the water sampling period. Lower panels show deuterium excess (dxs) of precipitation and (c) leaf area index (LAI) and (d) precipitation recycling (PR) accumulated along the back trajectories weighted by local precipitation for the water sampling period.

wet season may reflect the mixture of atmospheric processes and moisture sources providing different isotopic values. This notion is supported by the cluster analysis, which shows a large number of different circulation patterns during the wet season. Therefore, the results during this season remain somewhat inconclusive and need to be confirmed with further observations and isotope-enabled climate models.

Since the focus of this study is on dxs, the interannual variability was assessed, focusing on the most relevant parameters (LAI and PR) related with dxs, separating the wet and dry seasons and filling the gap from July to September 2016 with data from the Pomacochas station (Figure S5) as shown in Figure S6. Although there are only four values per year representing the seasonal averages, the consistent positive relationship during the dry season, which supports the notion of the positive relationship between forest activity and dxs, is worth noting.

4.2. Paleoclimate Implications

The antiphased behavior observed in the Holocene δ^{18}O record from speleothems from the eastern and western edges of the Amazon basin points to a see-saw effect in monsoon precipitation. On the one hand, this pattern is consistent with the variations in the intensity of the Bolivian-High-Nordeste Low system serving as the main driver of precipitation variability in the Amazon basin at orbital time scales (Cheng et al., 2013; Cruz et al., 2009). On the other hand, Wang et al. (2017) argue that upstream plant transpiration may bias the paleoclimate interpretation. In this scenario, the Holocene and Glacial rainfall stable isotopic composition over the western Amazon basin was to a large extent modulated by changes in forest evapotranspiration.
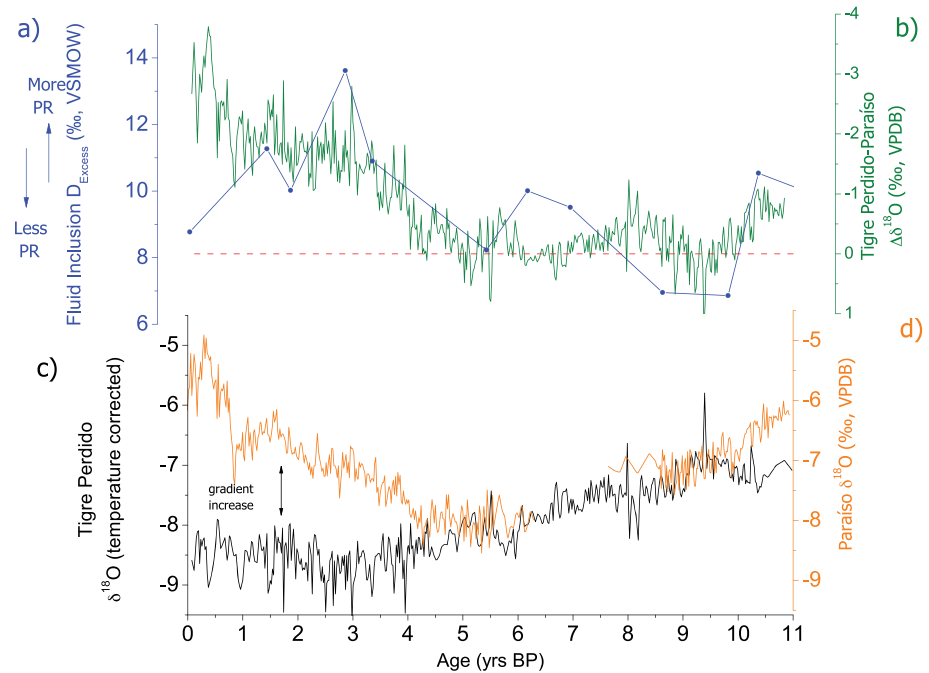
Figure 7. Comparison between stable isotope record from speleothems from the western and eastern Amazon edges: (a) dxs reconstruction from Tigre Perdido speleothem record (van Breukelen et al., 2008); (b) Tigre Perdido-Paraíso $\delta^{18}O$; (c) 20-year interpolated $\delta^{18}O$ record from Tigre Perdido cave speleothem (van Breukelen et al., 2008). The $\delta^{18}O$ values from Tigre Perdido are corrected by 1.4‰ to account for temperature variations between the caves following the procedure of Wang et al. (2017); (d) as in (c) but for 20-year interpolated $\delta^{18}O$ record from Paraíso cave speleothems (Wang et al., 2017).

Reconstructions of dxs based on fluid inclusions of speleothems from the western Amazon can provide important clues regarding moisture flux pathways and recycling processes. The calculated dxs from speleothem fossil drip water from Tigre Perdido cave in the western Amazon shows an antiphased behavior through the Holocene when compared with the $\delta^{18}O_{calcite}$ (Figures 7a and 7b) (van Breukelen et al., 2008). Although variations in moisture recycling can modulate the isotopic effect of DRU, they do not drastically change it; therefore, the antiphased response between dxs and $\delta^{18}O_{calcite}$ suggests that other processes besides the degree of rainout upstream drove the spatial changes in isotope variability during the Holocene. In other words, the east-west $\delta^{18}O$ dipole between the Paraíso and Tigre Perdido records sustained over thousands of years (Figures 7c and 7d) cannot be explained by an isotopic effect related to moisture recycling alone. It is noteworthy that the Holocene variations in dxs are similar to variations in the difference between $\delta^{18}O$ from the western and eastern edges of the Amazon basin, $\Delta\delta^{18}O_{Tigre\ Perdido-Paraíso}$. A negative $\Delta\delta^{18}O_{TigrePerdido-Paraíso}$ implies more negative rainfall $\delta^{18}O$ over the western Amazon (Tigre Perdido cave) compared to its eastern border (Paraíso cave). Assuming a common moisture flux pathway for both sites, the observed similarity in the absolute values of the $\delta^{18}O$ during the early to mid-Holocene cannot be explained by Rayleigh distillation processes alone. Indeed, if moisture reaching the western Amazon basin is the same as the one that passes over the central Amazon, the $\delta^{18}O$ values from the western border should always be slightly more negative than those from the eastern edge. Furthermore, during the same period, dxs values are lower, suggesting limited moisture recycling during winter. Moisture originating over the ocean and subject to only limited Rayleigh distillation is expected to be isotopically less negative and with almost similar isotopic composition over the western edge as over the central Amazon.

As we move toward the late Holocene, $\Delta\delta^{18}O_{TigrePerdido-Paraíso}$ becomes more negative as a result of more negative rainfall $\delta^{18}O$ over the western Amazon, concomitant with increased $\delta^{18}O$ values in the central-eastern Amazon. The dxs values from Tigre Perdido follow the same trend (Figure 7a and 7b). The high dxs recorded during the late Holocene points to an increase in moisture recycling associated with forest expansion, which allows for a greater contribution from winter precipitation fed by evapotranspirated forest moisture. The increasing trend in dxs along the Holocene is consistent with the increased rainforest pollen
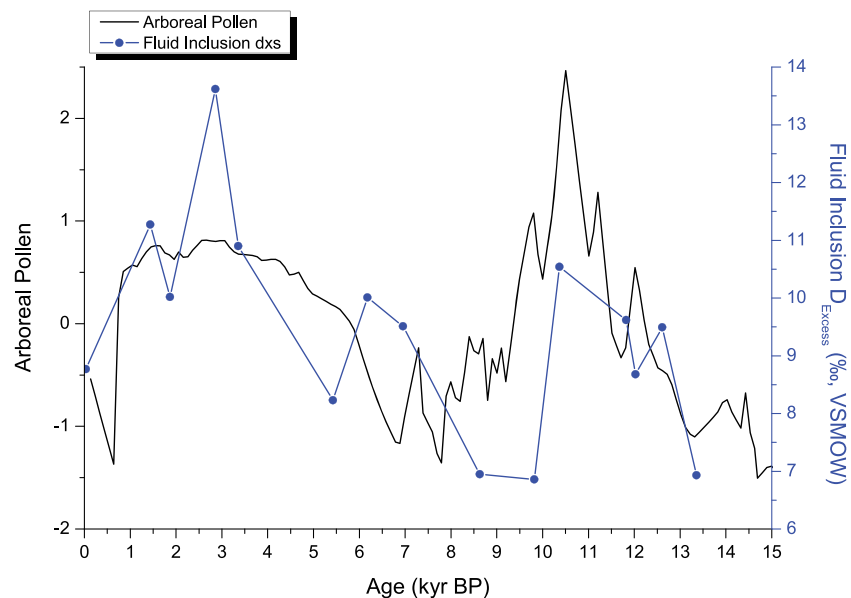
Figure 8. Comparison between calculated dxs from Tigre Perdido stalagmite (van Breukelen et al., 2008) with the integrated record of rainforest pollen frequency from three lakes: Laguna Chochos, Peru (Bush et al., 2005); Saci, central-south Amazon (Fontes et al., 2017); and Serra Sul Carajás Lake, CSS2 (Absy et al., 1991; Sifeddine et al., 2001).

frequency recorded in lakes from the south-central and eastern Amazon, supporting the notion of forest expansion during the middle and late Holocene (Fontes et al., 2017; Absy et al., 1991 ; Sifeddine et al., 2001) (Figures 8 and S2). Furthermore, the steep dxs increase observed from about 6 to 2 kyr BP agrees with numerical simulations of Amazon vegetation (Maksic et al., 2018), which show a clear expansion of the evergreen vegetation in the Amazon basin.

With the increase of the dxs values during the late Holocene, the difference between the absolute δ^{18}O values at Tigre Perdido and Paraiso also increases. This apparently contradicts Wang et al. (2017), which compare the Holocene with the upper Pleistocene, thereby contrasting conditions of fluctuating forest along the Holocene, with much less, or absence, of forest during the upper Pleistocene. However, our study focuses only on the Holocene, a period with more subtle variations and different conditions than the former study. Therefore, the establishment of a Rayleigh distillation mechanism across the forest that leads to significant $\Delta\delta^{18}O_{TigrePerdido-Paraíso}$ is likely in the presence of the forest, as observed when analyzing the winter isotopic composition in present-day rainfall.

5. Conclusions

We investigated the role of vegetation in driving changes in the rainfall isotopic composition in the western Amazon basin. As documented previously, the tropical North Atlantic and the Amazon rainforest are the main moisture sources for precipitation at the monitoring site (5.92°S, 77.35°W, 870 m. a. s. l.). Their moisture contributions vary seasonally with air parcel transport patterns, identified by means of cluster analysis of back trajectories. Precipitation derived from oceanic moisture with minimum exchange with surface evaporation has a less negative isotopic composition than precipitation originating from air parcels that travel over land and are affected by DRU through Rayleigh distillation. Furthermore, dxs at the monitoring site is a good indicator of the remote contribution to precipitation from forest evapotranspiration during the extended dry season (June to September). The relationship of dxs with δ^{18}O is sensitive to the exposure of the air mass to open forest, showing the best coupling between them when there is more exposure. Paleorecords show that during the early Holocene, the main moisture source to our monitoring site was located over the tropical North Atlantic and little moisture originated from land due to the reduced forest cover at the time, which probably limited water supply during the dry season. After the mid-Holocene,

the contribution from winter precipitation gains importance as the expansion of the forest permits more moisture recycling.

References

Absy, M. L., Cleef, A. M., Fournier, M., Martin, L., Servant, M., Sifeddine, A., et al. (1991). Mise en evidence de quatre phases d'ouverture de la foret dense dans le sudest del' Amazonie au cours de 60,000 dernieresannees. Premiere comparaison avec d'autres regions tropicales. *Comptes-Rendus de l'Académie des Sciences, Paris*, *312*, 673–678.

Apaéstegui, J., Cruz, F. W., Sifeddine, A., Vuille, M., Espinoza, J. C., Guyot, J. L., et al. (2014). Hydroclimate variability of the north-western Amazon Basin near the Andean foothills of Peru related to the South American Monsoon System during the last 1600 years. *Climateof the Past*, *10*(6), 1967–1981. https://doi.org/10.5194/cp-10-1967-2014

Baker, J. C. A., Gloor, M., Spracklen, D. V., Arnold, S. R., Tindall, J. C., Clerici, S. J., et al. (2016). What drives interannual variation in tree ring oxygen isotopes in the Amazon? *Geophysical Research Letters*, *43*, 11,831–11,840. https://doi.org/10.1002/2016GL071507

Builes-Jaramillo, A., & Poveda, G. (2018). Conjoint analysis of surface and atmospheric water balances in the Andes-Amazon system. *Water Resources Research*, *54*, 3472–3489. https://doi.org/10.1029/2017WR021338

Bush, M. B., Hansen, B. C. S., Rodbell, D. T., Seltzer, G. O., Young, K. R., León, B., Abbott, M. B.,et al. (2005). A 17 000-year history of Andean climate and vegetation change from Laguna de Chochos, Peru. *Journal of Quaternary Science*, *20*(7-8), 703–714. https://doi.org/10.1002/jqs.983

Chen, T., Weng, S., & Schubert, S. (1999). Maintenance of austral summertime upper-tropospheric circulation over tropical South America: The Bolivian high-Nordeste low system. *Journal of the Atmospheric Sciences*, *56*, 2081–2100.

Cheng, H., Sinha, A., Cruz, F. W., Wang, X., Edwards, R. L., d'Horta, F. M., et al. (2013). Climate change patterns in Amazonia and bio-diversity. *Nature Communications*, *4*(1), 1411. https://doi.org/10.1038/ncomms2415

Coplen, T. B. (2000). Laboratory information management system(LIMS) for light stable isotopes. U.S. *Geological SurveyOpen-File Report*, *00–345*, 121. http://water.usgs.gov/software/code/geochemical/lims/doc/ofr00345.pdf

Coplen, T. B., & Wassenaar, L. I. (2015). LIMS for Lasers 2015 for achieving long-term accuracy and precision of$\delta 2H, \delta 17O,$ and$\delta 18O$ of waters using laser absorption spectrometry. *Rapid Communications in Mass Spectrometry*, *29*(22), 2122–2130. https://doi.org/10.1002/rcm.7372

Cruz, F. W., Vuille, M., Burns, S. J., Wang, X., Cheng, H., Werner, M., et al. (2009). Orbitally driven east-west antiphasing of South American precipitation. *Nature Geoscience*, *2*(3), 210–214. https://doi.org/10.1038/ngeo444

Dansgaard, W. (1964). Stable isotopes in precipitation. *Tellus*, *16*, 436–468. https://doi.org/10.1111/j.2153-3490.1964.tb00181.x

Dee, D. P., Uppala, S. M., Simmons, A. J., Berrisford, P., Poli, P., Kobayashi, S.,et al.(2011). The ERA-Interim reanalysis: Configuration and performance of the data assimilation system. *Quarterly Journal of the Royal Meteorological Society*, *137*(656), 553–597. https://doi.org/10.1002/qj.828

Drumond, A., Marengo, J., Ambrizzi, T., Nieto, R., Moreira, L., & Gimeno, L. (2014). The role of the Amazon Basin moisture in the atmospheric branch of the hydrological cycle: A Lagrangian analysis. *Hydrology and Earth System Sciences*, *18*(2577–2598), 2014. https://doi.org/10.5194/hess-18-2577-2014

Espinoza, J. C., Ronchail, J., Lengaigne, M., Quispe, N., Silva, Y., Bettolli, M. L., et al. (2013). Revisiting wintertime cold air intrusions at the east of the Andes: Propagating features from subtropical Argentina to Peruvian Amazon and relationship with large-scale circulation patterns. *Climate Dynamics*, *41*(7-8), 1983–2002. https://doi.org/10.1007/s00382-012-1639-y

Farquhar, G. D., Cernusak, L. A., & Barnes, B. (2007). Heavy water fractionation during transpiration. *Plant Physiology*, *143*(1), 11–18. https://doi.org/10.1104/pp.106.093278

Fiorella, R. P., Poulsen, C. J., Zolá, R. S. P., Barnes, J. B., Tabor, C. R., & Ehlers, T. A. (2015). Spatiotemporal variability of modern precipitation $\delta^{18}O$ in the central Andes and implications for paleoclimate and paleoaltimetry estimates. *Journal of Geophysical Research: Atmospheres*, *120*, 4630–4656. https://doi.org/10.1002/2014JD022893

Fisch, G., Tota, J., Machado, L. A. T., Dias, M. S., Lyra, R. D. F., Nobre, C. A., et al. (2004). The convective boundary layer over pasture and forest in Amazonia. *Theoretical and Applied Climatology*, *78*, 47–59.

Fontes, D., Cordeiro, R. C., Martins, G. S., Behling, H., Turcq, B., Sifeddine, A., et al. (2017). Paleoenvironmental dynamics in South Amazonia, Brazil, during the last 35,000 years inferred from pollen and geochemical records of Lago do Saci. *Quaternary Science Reviews*, *173*, 161–180. https://doi.org/10.1016/j.quascirev.2017.08.021

Froehlich, K., Gibson, J. J., & Aggarwal, P. (2002). Deuterium excess in precipitation and its climatological significance, in: Study of Environmental Change Using Isotope Techniques. *International Atomic Energy Agency, Vienna*, *54–66*, 2002.

Gat, J. R., Bowser, C. J., & Kendall, C. (1994). The contribution of evaporation from the Great Lakes to the continental atmosphere: Estimate based on stable isotope data. *Geophysical Research Letters*, *21*, 557–560. https://doi.org/10.1029/94gl00069

Griffis, T. J., Sargent, S. D., Lee, X., Baker, J. M., Greene, J., Erickson, M., et al. (2010). Determining the oxygen isotope composition of evapotranspiration using eddy covariance. *Boundary-Layer Meteorology*, *137*(2), 307–326. https://doi.org/10.1007/s10546-010-9529-5

Houze, R. A. Jr. (1993). *Cloud dynamics*, *573*. San Diego, Calif.: Academic.

Huffman, G. J., Bolvin, D. T., Nelkin, E. J., Wolff, D. B., Adler, R. F., Gu, G., et al. (2007). The TRMM Multisatellite Precipitation Analysis (TMPA): Quasi-global, multiyear, combined-sensor precipitation estimates at fine scales. *Journal of Hydrometeorology*, *8*, 38–55. https://doi.org/10.1175/JHM560.1

Hurley, J. V., Galewsky, J., Worden, J., & Noone, D. (2012). A test of the advection-condensation model for subtropical water vapor using stable isotopologue observations from Mauna Loa Observatory, Hawaii. *Journal of Geophysical Research*, *117*, D19118. https://doi.org/10.1029/2012JD018029

Hurley, J. V., Vuille, M., Hardy, D. R., Burns, S., & Thompson, L. G. (2015). Cold air incursions, $\delta^{18}O$ variability and monsoon dynamics associated with snow days at Quelccaya Ice Cap, Peru. *Journal of Geophysical Research: Atmospheres*, *120*, 7467–7487. https://doi.org/10.1002/2015JD023323

Insel, N., Poulsen, C. J., Sturm, C., & Ehlers, T. A. (2013). Climate controls on Andean precipitation $\delta^{18}O$ interannual variability. *Journal of Geophysical Research: Atmospheres*, *118*, 9721–9742. https://doi.org/10.1002/jgrd.50619

Konecky, B. L., Noone, D. C., & Cobb, K. M. (2019). The influence of competing hydroclimate processes on stable isotope ratios in tropical rainfall. *Geophysical Research Letters*, *46*, 1622–1633. https://doi.org/10.1029/2018GL080188

Koster, R. D., Valpine, D. P., & Jouzel, J. (1993). Continental water recycling and $H_2^{18}O$ concentrations. *Geophysical Research Letters*, *20*, 2215–2218.

Lachniet, M. S. (2009). Climatic and environmental controls on speleothem oxygen-isotope values. *Quaternary Science Review*, *28*, 412–432. https://doi.org/10.1016/j.quascirev.2008.10.021

Landais, A., Risi, C., Bony, S., Vimeux, F., Descroix, L., Falourd, S., & Bouygues, A. (2010). Combined measurements of 17O-excess and d-excess in African monsoon precipitation: Implications for evaluating convective parameterizations. *Earth and Planetary Science Letters*, *298*, 104–112.

Lenters, J. D., & Cook, K. H. (1997). On the origin of the Bolivian high and related circulation features of the South American climate. *Journal of the Atmospheric Sciences*, *54*, 656–678. https://doi.org/10.1175/1520-0469(1997)054b0656:OTOOTBN2.0.CO;2

Lenters, J. D., & Cook, K. H. (1999). Summertime precipitation variability over South America: Role of the large-scale circulation. *Monthly Weather Review*, *127*, 409–431.

Maksic, J., Shimizu, M. H., De Oliveira, G. S., Venancio, I. M., Cardoso, M., & Ferreira, F. A. (2018). Simulation of the Holocene climate over South America and impacts on the vegetation. *The Holocene*, *29*(2), 287–299. https://doi.org/10.1177/0959683618810406

Mayta, V. C., Ambrizzi, T., Espinoza, J. C., & Silva Dias, P. L. (2019). The role of the Madden–Julian oscillation on the Amazon Basin intraseasonal rainfall variability. *International Journal of Climatology*, *39*(1), 343–360. https://doi.org/10.1002/joc.5810

Molina, R. D., Salazar, J. F., Martínez, J. A., Villegas, J. C., & Arias, P. A. (2019). Forest-induced exponential growth of precipitation along climatological wind streamlines over the Amazon. *Journal of Geophysical Research: Atmospheres*, *124*, 2589–2599. https://doi.org/10.1029/2018JD029534

Myneni, R., Knyazikhin, Y., & Park, T. (2015). MCD15A2H MODIS/Terra+Aqua Leaf Area Index/FPAR 8-day L4 Global 500m SIN Grid V006. *NASA EOSDIS Land Processes DAAC*. http://doi.org/10.5067/MODIS/MCD15A2H.006

Morton, D. C., Nagol, J., Carabajal, C. C., Rosette, J., Palace, M., Cook, B. D., et al.. (2014). Amazon forests maintain consistent canopy structure and greenness during the dry season. *Nature*, *506*(7487), 221–224. https://doi.org/10.1038/nature13006

Myneni, R. B., Yang, W., Nemani, R. R., Huete, A. R., Dickinson, R. E., Knyazikhin, Y., et al. (2007). Large seasonal swings in leaf area of Amazon rainforests. *Proceedings of the National Academy of Sciences*, *104*(12), 4820–4823. https://doi.org/10.1073/pnas.0611338104

Numaguti, A. (1999). Origin and recycling processes of precipitating water over the Eurasian continent: Experiments using an atmospheric general circulation model. *Journal of Geophysical Research: Atmospheres*, *104*(D2), 1957–1972. https://doi.org/10.1029/1998jd200026

Paccini, L., Espinoza, J. C., Ronchail, J., & Segura, H. (2017). Intra-seasonal rainfall variability in the Amazon basin related to large-scale circulation patterns: A focus on western Amazon–Andes transition region. *International Journal of Climatology*, *38*, 2386–2399. https://doi.org/10.1002/joc.5341

Peng, H., Mayer, B., Harris, S., & Krouse, H. (2007). The influence of below-cloud secondary effects on the stable isotope composition of hydrogen and oxygen in precipitation at Calgary, Alberta, Canada. *Tellus B*, *59*, 698–704. https://doi.org/10.1111/j.1600-0889.2007.00291.x

Pfahl, S., & Sodemann, H. (2014). What controls deuterium excess in global precipitation? *Climate of the Past*, *10*(771–781), 2014. https://doi.org/10.5194/cp-10-771-2014

Risi, C., Landais, A., Winkler, R., & Vimeux, F. (2013). Can we determine what controls the spatio-temporal distribution of d-excess and 17O-excess in precipitation using the LMDZ general circulation model? *Climate of the Past*, *9*, 2173–2193.

Rolph, G., Stein, A., & Stunder, B. (2017). Real-time Environmental Applications and Display sYstem: READY. *Environmental Modelling & Software*, *95*, 210–228. https://doi.org/10.1016/j.envsoft.2017.06.025

Rozanski, K., Araguás-Araguás, L., & Gonfiantini, R. (1993). *Isotopic patterns in modern global precipitation. Climate Change in Continental Isotopic Records, Geophysical Monograph*, (Vol. 78, pp. 1–36). Washington DC: American Geophysical Union.

Salati, E., Dall'Olio, A., Matsui, E., & Gat, J. R. (1979). Recycling of water in the Amazon Basin: An isotopic study. *Water Resources Research*, *15*, 1250–1258. https://doi.org/10.1029/WR015i005p01250

Saleska, S. R., Wu, J., Guan, K., Araujo, A. C., Huete, A., Nobre, A. D., & Restrepo-Coupe, N. (2016). Dry-season greening of Amazon forests. *Nature*, *531*(7594), E4–E5. https://doi.org/10.1038/nature16457

Samuels-Crow, K. E., Galewsky, J., Hardy, D. R., Sharp, Z., Worden, J., & Braun, C. (2014). Upwind convective influences on the isotopic composition of atmospheric water vapor over the tropical Andes. *Journal of Geophysical Research: Atmospheres*, *119*, 7051–7063. https://doi.org/10.1002/2014JD021487

Schwarcz, H. P., Harmon, R. S., Thompson, P., & Ford, D. C. (1976). Stable isotope studies of fluid inclusions in speleothems and their paleoclimatic significance. *Geochimica et Cosmochimica Acta*, *40*, 657–665.

Segura, H., Junquas, C., Espinoza, J. C., Vuille, M., Jauregui, Y. R., Rabatel, A., et al. (2019). New insights into the rainfall variability in the tropical Andes on seasonal and interannual time scales. *Climate Dynamics*, *53*(1-2), 405–426. https://doi.org/10.1007/s00382-018-4590-8

Sifeddine, A., Martin, L., Turcq, B., Ribeiro, C. V., Soubies, F., Cordeiro, R. C., & Suguio, K. (2001). Variations of the Amazonian rainforest environment: A sedimentological record covering 30,000 years. *Palaeogeography, Palaeoclimatology, Palaeoecology*, *168*, 221–235.

Sörensson, A. A., & Ruscica, R. C. (2018). Intercomparison and Uncertainty Assessment of Nine Evapotranspiration Estimates Over South America. *Water Resources Research*, *54*(4), 2891–2908. https://doi.org/10.1002/2017wr021682

Staal, A., Tuinenburg, O. A., Bosmans, J. H. C., Holmgren, M., van Nes, E. H., Scheffer, M., et al. (2018). Forest-rainfall cascades buffer against drought across the Amazon. *Nature Climate Change*, *8*(6), 539–543. https://doi.org/10.1038/s41558-018-0177-y

Stein, A. F., Draxler, R. R., Rolph, G. D., Stunder, B. J. B., Cohen, M. D., & Ngan, F. (2015). NOAA's HYSPLIT Atmospheric Transport and Dispersion Modeling System. *Bulletin of the American Meteorological Society*, *96*(12), 2059–2077. https://doi.org/10.1175/bams-d-14-00110.1

Sulca, J., Vuille, M., Silva, Y., & Takahashi, K. (2016). Teleconnections between the Peruvian central Andes and Northeast Brazil during extreme rainfall events in austral summer. *Journal of Hydrometeorology*, *17*, 499–515.

Sylvestre, F., Servant, M., Servant-Vildary, S., Causse, C., Fournier, M., & Ybert, J.-P. (1999). Lake-level chronology on the southern Bolivian Altiplano (18°–23°S) during Late-Glacial time and the early Holocene. *Quaternary Research*, *51*, 54–66.

Van Breukelen, M. R., Vonhof, H. B., Hellstrom, J. C., Wester, W. C. G., & Kroon, D. (2008). Fossil dripwater in stalagmites reveals Holocene temperature and rainfall variation in Amazonia. *Earth and Planetary Science Letters*, *275*(1-2), 54–60. https://doi.org/10.1016/j.epsl.2008.07.060

Van der Ent, R. J. (2014). A new view on the hydrological cycle over continents, Ph.D. thesis, 96 pp, Delft University of Technology, Delft. https://doi.org/10.4233/uuid:0ab824ee-6956-4cc3-b530-3245ab4f32be.

Vera, C., Higgins, W., Amador, J., Ambrizzi, T., Garreaud, R., Gochis, D., et al. (2006). Toward a unified view of the American monsoon systems. *Journal of Climate*, *19*(20), 4977–5000. https://doi.org/10.1175/JCLI3896.1

Villacís, M., Vimeux, F., & Taupin, J. D. (2008). Analysis of the climate controls on the isotopic composition of precipitation (δ18O) at Nuevo Rocafuerte, 74.5°W, 0.9°S, 250m, Ecuador. *Comptes Rendus Geoscience*, *340*(1), 1–9. https://doi.org/10.1016/j.crte.2007.11.003

Vimeux, F., Gallaire, R., Bony, S., Hoffmann, G., & Chiang, J. C. H. (2005). What are the climate controls on δD in precipitation in the Zongo Valley (Bolivia)? Implications for the Illimani ice core interpretation. *Earth and Planetary Science Letters*, *240*, 205–220. https://doi.org/10.1016/j.epsl.2005.09.031

Vuille, M. (2018). Current state and future challenges in stable isotope applications of the tropical hydrologic cycle *(Invited Commentary)*. *Hydrological Processes*, *32*, 1313–1317. https://doi.org/10.1002/hyp.11490

Vuille, M., & Werner, M. (2005). Stable isotopes in precipitation recording South American summer monsoon and ENSO variability—Observations and model results. *Climate Dynamics*, *25*, 401–413. https://doi.org/10.1007/s00382-005-0049-9

Wackerbarth, A., Langebroek, P. M., Werner, M., Lohmann, G., Riechelmann, G., Borsato, A., & Mangini, A. (2012). Simulated oxygen isotopes in cave drip water and speleothem calcite in European caves. *Climate of the Past*, *8*, 1781–1799. https://doi.org/10.5194/cp-8-1781-2012

Wang, L., Good, S. P., Caylor, K. K., & Cernusak, L. A. (2012). Direct quantification of leaf transpiration isotopic composition. *Agricultural and Forest Meteorology*, *154-155*, 127–135. https://doi.org/10.1016/j.agrformet.2011.10.018

Wang, X., Edwards, R. L., Auler, A. S., Cheng, H., Kong, X., Wang, Y., et al. (2017). Hydroclimate changes across the Amazon lowlands over the past 45,000 years. *Nature*, *541*(7636), 204–207. https://doi.org/10.1038/nature20787

Windhorst, D., Waltz, T., Timbe, E., Frede, H.-G., & Breuer, L. (2013). Impact of elevation and weather patterns on the isotopic composition of precipitation in a tropical montane rainforest. *Hydrology and Earth System Sciences*, *17*, 409–419. https://doi.org/10.5194/hess-17-409-2013

Zemp, D. C., Schleussner, C.-F., Barbosa, H. M. J., van der Ent, R. J., Donges, J. F., Heinke, J., et al.(2014). On the importance of cascading moisture recycling in South America. *Atmospheric Chemistry and Physics*, *14*(23), 13337–13359. https://doi.org/10.5194/acp-14-13337-2014

Zimmermann, U., Ehhalt, D., & Muennich, K. O. (1967). Soil-water movement and evapotranspiration: Changes in the isotopic composition of the water. *International Atomic Energy Agency (IAEA): IAEA*.

Zhou, J., & Lau, K.-M. (1998). Does a monsoon climate exist over South America? *Journal of Climate*, *11*, 1020–1040. https://doi.org/10.1175/1520-0442(1998)011<1020:DAMCEO>2.0.CO;2